Speeds of Sound in Binary Mixtures of Water and Carbon Dioxide at Temperatures from 273 K to 313 K and at Pressures up to 50 MPa

Subash Dhakal[1] · Saif Z. S. Al Ghafri[1] · Darren Rowland[1] · Eric F. May[1] · J. P. Martin Trusler[2] · Paul L. Stanwix[1]

Abstract

Knowledge of thermodynamic properties of aqueous solutions of CO_2 is crucial for various applications including climate science, carbon capture, utilisation and storage (CCUS), and seawater desalination. However, there is a lack of reliable experimental data, and the equation of state (EOS) predictions are not reliable, particularly for sound speeds in low CO_2 concentrations typical of water resources. For this reason, we have measured speeds of sound in three different aqueous solutions containing CO_2. We report speeds of sound in the single-phase liquid region for binary mixtures of water and CO_2 for mole fractions of CO_2 of 0.0118, 0.0066 and 0.0015 at temperatures from 273.15 K to 313.15 K and at pressures up to 50 MPa, measured using a dual-path pulse-echo apparatus. The relative standard uncertainties of the sound speeds are 0.05 %, 0.03 % and 0.01 % at 0.0118, 0.0066 and 0.0015 CO_2 mole fractions, respectively. The change in sound speeds as functions of composition, pressure and temperature are analysed in this study. We find that dissolution of CO_2 in water increases its sound speeds at all conditions, with the greatest increase occurring at the highest mole fractions of CO_2. Our sound speed data agree well with the limited available experimental data in the literature but deviate from the EOS-CG of Gernert and Span by up to 7 % at the lowest temperatures, highest pressures, and highest CO_2 mole fraction. The new low-uncertainty sound speed data presented in this work could provide a basis for development of an improved EOS and in establishing reliable predictions of the change in thermodynamic properties of seawater-like mixtures due to absorption of CO_2 gas.

Keywords Carbon dioxide · CCUS · Climate change · Pulse echo · Seawater thermodynamics · Speed of sound

---

Extended author information available on the last page of the article

⚛ Springer

1 Introduction

Accurate description of the thermodynamic properties of aqueous CO_2 solutions is crucial to understanding the effects of anthropogenic CO_2 emissions on the earth's oceans and hence the climate system [1]. Carbon capture, utilisation, and storage (CCUS) processes, which are aimed at reducing the emissions of CO_2 into the atmosphere by means of geological storage, also require accurate understanding of the thermodynamic properties of CO_2 aqueous solutions [2]. Other important applications of the knowledge of thermodynamic properties of these solutions include seawater desalination and waste water treatment, among others [1]. Seawater desalination is a critical process ensuring access of potable water to millions of people and sustaining livelihoods of over 300 million people world-wide [3, 4]. Similarly, waste water treatment involves the removal of harmful pathogens, malodorous gases, inorganic salts, hazardous chemicals, etc. from residential and industrial waste water so that cleaner and safer water can be discharged into the water bodies [5]. To characterise systematically the effect of dissolved CO_2 on the thermodynamic properties of seawater-like mixtures, we first focus our attention on understanding the effects of CO_2 absorption by pure water at pressure and temperature conditions representative of those available in oceans, at low CO_2 mole fraction of up to 0.01 (close to the saturation concentration of CO_2 in standard seawater) [6]. (Our future research will extend this work to saline solutions with absorbed CO_2.)

The uncertainty associated with long-term climate predictions is one of the greatest challenges to developing strategies for mitigating the impact of climate change [7]. For example, one of the key metrics used to describe the effects of climate change, the global mean surface temperature (GMST), is estimated to be somewhere between 2 °C and 4.5 °C with a recent study indicating that it could be higher than 5 °C [8]. A major source of uncertainty can be linked to the uncertainty in the evaluation of the effective heat capacity used in climate models, which in turn is dominated by the heat capacity of oceans [9]. Therefore, predictions of the global ocean heat capacity and the resulting change in heat capacity due to the absorption of the ever-increasing anthropogenic CO_2 emissions become vitally important. In situ measurement of the thermodynamic properties of oceans is practically impossible and the reliability of available equations-of-state for predicting the thermodynamic properties, particularly for the $CO_2 + H_2O$ system, cannot be assessed based on available experimental data. The only comprehensive fundamental equation of state for this system, that of Gernert and Span [10], is based largely on the properties of humid gases and CO_2-rich mixtures, particularly at higher mole fractions of CO_2. While there are abundant density and solubility data available in the literature for this system, heat capacity and sound speed data are scare; only one research article [11] with few data points on sound speeds at very low-pressure conditions was identified in the course of this work. A selection of the available density, heat capacity and solubility data are provided in Table 1.

Direct laboratory measurements of the heat capacity, density, compressibility and other thermophysical properties are challenging at the high pressures found in deep ocean environments. An alternative and accurate approach is to measure the sound

Table 1 Selected literature thermodynamic property and solubility data of $xCO_2 + (1-x) \cdot H_2O$ mixtures

References	Year	N*	x^a	T/K	p/MPa	u^b (%)
Density						
Nighswander [12]	1989	33	0.002–0.016	353–473	2–10	0.4
Fenghour [13]	1996	104	0.0612–0.7913	415–645	5.9–28	0.08–0.14
Hnedkovsky [14]	1996	32	0.003–0.004	298–705	1–35	0.1
Song [15]	2003	33	0–0.061	273–284	5–12.5	–
Zhaowen [16]	2004	6	0.018	332	0.3–29	0.01
Hebach [17]	2004	164	Saturation	284–333	1–30	0.15
McBride-Wright [18]	2015	91	0.0086–0.0271	294–449	15–100	0.035
Efika [19]	2016	290	Saturation	293–450	1.45–64	0.1–1
Heat capacity						
Barbero [20]	1983	10	0.0002–0.002	298	0.1	–
Hnedkovsky [21]	1997	15	0.003	304–704	28	–
Solubility						
Nighswander [12]	1989	33	–	353–473	2–10	1–4
Teng [22]	1997	24	–	278–293	6.4–29.5	1.6
Servio [23]	2001	9	–	277–283	2–4.2	3–5
Anderson [24]	2002	54	–	274–288	0.1–2.2	1
Zhaowen [16]	2004	6	–	332	3–20	2

[a]Mole fraction of CO_2 in the mixture

[b]Reported Standard Uncertainty

*Number of points measured

speeds in a fluid solution or mixture of interest, which along with few reference density and heat capacity values can be used to evaluate other relevant thermodynamic properties across the experimental range of conditions [25]. This study focuses on the experimental determination of sound speeds in the $CO_2 + H_2O$ system at temperatures from $T = 273.15$ K to 313.15 K and pressures up to 50 MPa, conditions which are typical of oceans. To mimic the low concentrations of CO_2 expected to occur in the oceans, mole fractions of $x = 0.0118$, 0.0066 and 0.0015 are considered in this study. At these concentrations of CO_2, the solutions remain well within the single-phase state, based on the solubility model predictions of Duan et al. [26]. The measurement regime of our study is illustrated in Fig. 1.

2 Apparatus and Materials

Sound speeds were measured using a dual-path pulse-echo apparatus, comprising a measurement cell fabricated out of 316 stainless steel, operating at 10 MHz, and housed within a high-pressure vessel (HPV) as shown in Fig. 2. The apparatus was purpose-built for these experiments, but is similar in design to one described previously to measure sound speeds in p-xylene [27] and toluene [25]. The unique
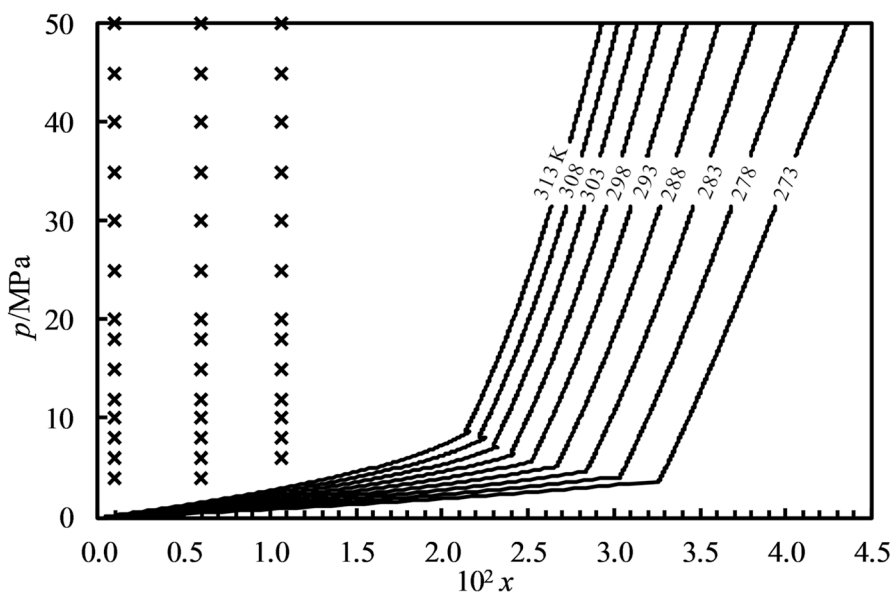
Fig. 1 p–x diagram showing solubility isotherms calculated using the CO2 solubility model of Duan et al. [26]. The cross symbols represent the state points where sound speed measurements were made for all three mixtures in this study at temperatures from 273 K to 313 K
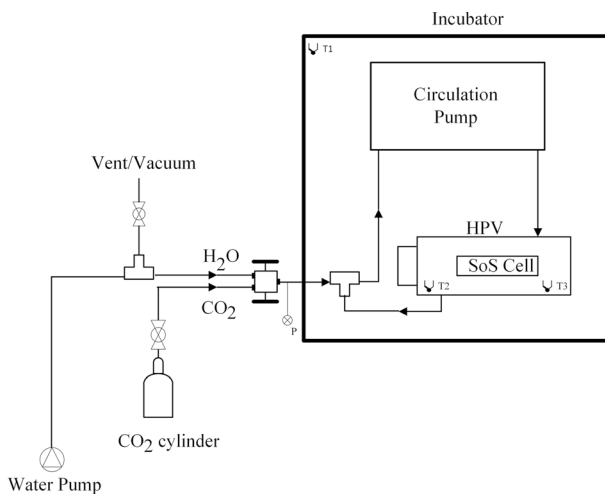

Fig. 2 Schematic of experimental apparatus for the measurement of sound speeds in binary H_2O and CO_2 mixtures

features of the apparatus used in this work were the incorporation of a recirculating pump, for in situ mixing of the solution, and that the piezo-ceramic transducer element of the sensor was encapsulated in polyimide (supplied by PI Ceramic GmbH), to isolate both anode and cathode from the fluid. The HPV and circulation pump

were housed inside an incubator (Memmert ICP110eco) with an operational range of $-12\,°C$ to $+60\,°C$ and temperature stability of $0.1\,°C$. CO_2 and water could be injected into the system via a three-way valve, located outside the incubator and connected to the recirculation loop through a tee connector. Pure CO_2 was fed directly into the system from a pressure-regulated cylinder. Degassed pure water was injected into the system using a pressure-controlled high-pressure syringe pump (Teledyne ISCO, 260D).

Two platinum resistance thermometer (PRT) probes (Netsushin, NR–141–100S–1–1.6–18–2500PLi (Φ 0.2)–A–MC–1205) monitored the wall temperature of the HPV, with each located at the ends of the cell to monitor the temperature uniformity and provide an average cell temperature. These PRTs were calibrated against a standard platinum resistance thermometer, WIKA CTR5000 having a standard uncertainty of 1 mK, with model CTS500 multiplexer between 258.15 K and 373.15 K and fitted to the Callendar-Van Dusen equation with temperature uncertainty of 8.5 mK. Considering the calibration uncertainty, the fluctuations and drift in incubator temperature as well as non-uniformity of temperature across the cell, the overall standard uncertainty in experimental temperature measurements reported in this work was evaluated to be 20 mK.

The system pressure was monitored using a piezoresistive pressure transmitter (Keller, PA-33X) located immediately outside the incubator, with an operational range of 100 MPa with a manufacturer specified expanded uncertainty of 0.05 % full scale. The pressure transducer calibration and performance were validated (Australian Pressure Laboratory), with a reported measurement uncertainty of 0.01 %.

The chemical samples used in this study are provided in Table 2.

The reader is referred to our previous publications for details on the design and operation of the apparatus as well as the data acquisition and signal processing techniques [25, 27, 28]. Briefly, the speed of sound was determined by generating an acoustic pulse within the sensor, then measuring the difference in arrival time, Δt, between two echoes that travel different paths with a known difference in path length, ΔL. The sound speed, c, is evaluated using the relation,

$$c = \frac{2\Delta L}{\Delta t}. \tag{1}$$

In this work a 10-cycle sinusoidal tone burst was used, and the results reported represent an average of at least 5 measurements of time delay, with maximum relative standard deviations of less than 0.01 %. The design of the sensor used in this

Table 2 Description of chemical samples used in the study where x is mole fraction purity, w is mass-fraction purity and ρ_e is the electrical resistivity

Chemical name	CAS number	Source	Purity x	Additional Purification
Carbon dioxide	124-38-9	BOC	0.99995	None
Water	7732-18-5	Ibis Technology	$\rho_e \geq 18$ MΩ·cm at $T = 298$ K	Degassed under vacuum
NaCl	7647-14-5	Chem-supply	$w \geq 0.997$	None

work is based on the work by Ball and Trusler [28] for which the diffraction corrections are less than 0.01 % of the measured time difference and thus can be neglected.

3 Calibrations and Validation

Calibration of the path length difference was carried out by measuring sound speeds in pure water at four temperatures, $T = 273.15$ K, 283.15 K, 298.15 K and 313.15 K and comparing the results to the values predicted using IAPWS-95 [29]. An average path length difference of $2\Delta L_0 = 19.901$ mm was obtained with an uncertainty $u(2\Delta L_0) = 0.001$ mm at a reference pressure of $p_0 = 0.1$ MPa and reference temperature of $T_0 = 298.15$ K.

The calibrated path length difference was extended to the entire experimental domain by means of the following relation:

$$2\Delta L(T, p) = 2\Delta L_0 \left(1 + \alpha(T - T_0) - 1/3\beta(p - p_0)\right), \tag{2}$$

where α is the linear thermal expansivity and β is the isothermal compressibility of 316 stainless steel, the latter considered constant over the ranges of temperature and pressure investigated. In this work, α was represented by a temperature-dependent function fitted to experimental thermal-expansion measurements of a sample of stock material, carried out by National Physical Laboratory (NPL), UK. The value of β was evaluated by fitting the bulk modulus data of Hammond et al. [30], Ledbetter [31], Grujicic and Zhao [32].

The experimental sound speed measurements in water are compared against the literature data of Lin and Trusler [33] with the IAPWS-95 EOS [29] as baseline in Fig. 3. Our data are consistent with the IAPWS-95 predictions within its reported uncertainties. Maximum deviations of our data from the IAPWS-95 EOS are 0.07 % at $T = (273 \text{ and } 283)$ K and 0.02 % at $T = (298 \text{ and } 313)$ K, while the EOS reported uncertainties are 0.1 % and 0.05 %, respectively in these conditions. Similarly, the low-uncertainty experimental sound speeds reported by Lin and Trusler [29] show good agreement with our data.

Fig. 3 Relative percentage deviations of the experimental speed of sound data in pure water, c_{exp}, from the IAPWS-95 [29] sound speeds, c_{EOS}. This work: ○, $T = 273.17$ K; □, $T = 283.20$ K; △, $T = 298.25$ K; ×, $T = 313.32$ K; Lin and Trusler [33]: ●, $T = 273.21$ K; ■, $T = 293.16$ K; ▲, $T = 313.16$ K
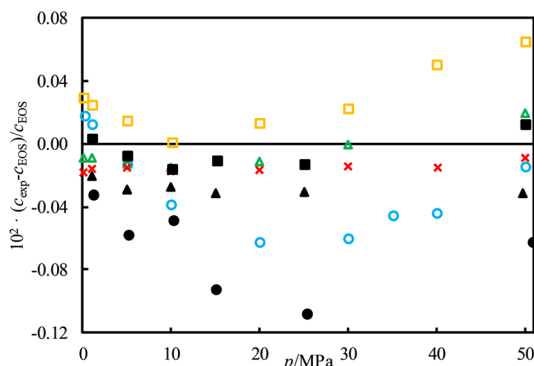
Calibration of the system volume was performed using water and CO_2. To calibrate the volume, the entire system was first evacuated, then the fluid (degassed water or CO_2) was injected into the system using a high-pressure syringe pump, taking note of the initial and final pump volumes. After subtracting dead volumes and accounting for pressurisation of the system, a final volume of 46.26 ml was obtained with a standard uncertainty of 0.05 ml.

To further validate the apparatus, measurements of sounds speeds in binary mixture of NaCl and water were carried out (see Table 3) and compared against the correlation of Chen et al. [34]. A mixture with molality $m = 0.5020$ mol·kg^{-1} was prepared gravimetrically by dissolving NaCl into vacuum-degassed pure water. The mixture was then injected into the system using the high-pressure syringe pump and measurements were taken at temperatures $T = 278.22$ K, 288.25 K and 298.31 K and pressures between 10 MPa and 40 MPa. Results of comparisons against the correlation of Chen et al. [34] are presented graphically in Fig. 4. Their reported uncertainty of 0.15 m·s^{-1} in relative sound speed (versus water) corresponds to a relative standard uncertainty of nearly 0.4 % under these conditions. Our measurements agree well with the predictions of the correlation,

Table 3 Measured speeds of sound c and combined standard uncertainty $u_c(c)$ as a function of pressure p and temperature T in brine, where $m = 0.5020$ mol·kg^{-1}

T/K	p/MPa	c/(m·s^{-1})	$u_c(c)$ /(m·s^{-1})
278.22	9.97	1481.03	0.13
278.20	10.00	1480.92	0.13
278.21	19.95	1497.46	0.14
278.22	29.92	1514.09	0.14
278.22	40.00	1531.28	0.14
278.22	40.00	1531.20	0.14
288.18	9.99	1517.03	0.13
288.24	9.99	1517.16	0.13
288.25	19.97	1533.74	0.13
288.25	29.97	1550.39	0.14
288.24	30.02	1550.52	0.14
288.25	39.99	1567.16	0.14
298.30	10.01	1545.44	0.13
298.31	20.00	1562.13	0.13
298.31	29.99	1578.88	0.14
298.31	39.98	1595.47	0.14
298.31	40.02	1595.45	0.14

Standard uncertainty of temperature $u(T)$: 20 mK, standard uncertainty of pressure, $u(p) = 8$ kPa and standard uncertainty of NaCl brine composition, $u(b) = 0.0015$ mol·kg^{-1}

Fig. 4 Relative percentage deviations of the experimental sound speeds in brine with a molality of $m = 0.5020$ mol·kg^{-1}, c_{exp}, from the correlation of Chen et al. [34], c_{corr}. $\bigcirc$, $T = 278.22$ K; $\square$, $T = 288.18$ K; $\triangle$, $T = 298.31$ K
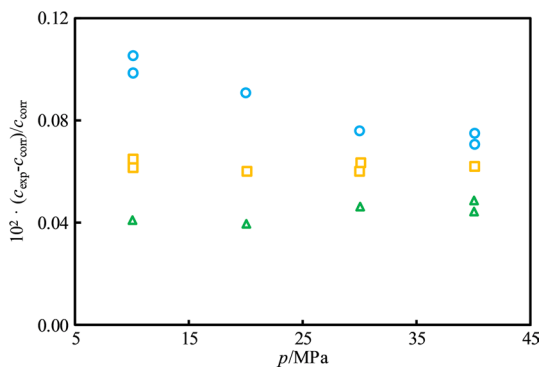
with maximum deviations of less than 0.11 % and average deviations of about 0.07 % falling well below their uncertainty.

4 Mixture Preparation

To prepare the mixture, CO_2 and water were sequentially injected into the evacuated system (comprising the sensor and circulation pump, described above) and mixed in situ using the circulation pump. Firstly, the required amount of CO_2, calculated using the calibrated system volume and density predicted from the equation-of-state of Span and Wagner [35], was slowly injected into the evacuated system by monitoring the system pressure. The CO_2 inlet valve was closed when the desired pressure was reached, at a temperature of $T = 298.15$ K inside the temperature-controlled incubator. The system was then left to stabilize for about 1–2 h. As an example, for the $x = 0.01$ composition, a pressure of about $p = 1.2$ MPa was maintained inside the system. Secondly, pure water was degassed under vacuum using a magnetic stirrer for more than 2 h, then pressurised for injection using a high-pressure syringe pump. A constant pressure of $p = 10$ MPa was maintained inside the pump with the water present up to the 3-way valve at the system inlet. The volume of water inside the pump at this stage was noted along with the pump temperature. The inlet valve was then slightly opened, allowing water to slowly move into the system at a flow rate of 0.5 ml/ min. As water was injected into the system, the circulation pump was operated to continuously mix the water and CO_2. A homogeneous mixture was achieved when the overall system pressure and high-pressure syringe pump volume remained stable for 1 h, typically after around 8 h. The final volume of the pump was recorded to determine the total amount of injected water. For the target $x = 0.01$ mol fraction, the actual composition prepared was $x = 0.0118$. This process is illustrated in Fig. 5 in which the increase in system pressure is plotted alongside the decrease in the pump volume as functions of time in hours during the $x = 0.0118$ mixture preparation.

Prior to the preparation and measurement of each mixture, the system was cleaned by removing any remaining sample through the vent line by repeatedly pressurising the system with helium and then venting, until water was no longer visible through

Fig. 5 Variation of system pressure, p (— —) and pump volume Vpump ($\cdots$), over time as water is injected into the system containing CO_2 with circulation pump in operation during $x=0.0118$ mixture preparation
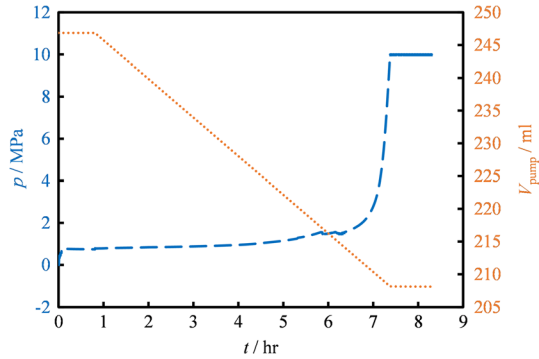
the vent line. After this, the system was evacuated for a minimum of 24 h at elevated temperature ($T=333.15$ K). To ensure there was no moisture trapped into the system, helium was again used to flush the system and the system was vacuumed again for at least another 24 h before the next mixture was prepared for measurement.

The uncertainty in the mole fraction of CO_2, x, was evaluated using the relation given in Eq. 3 [36],

$$u(x) = x(1-x)\left[\left(u_r(\rho_L)\right)^2 + \left(u_r(\rho_G)\right)^2 + \left(u_r(V_L)\right)^2 + \left(u_r(V_G)\right)^2\right]^{1/2}, \quad (3)$$

where L and G subscripts refer to water and CO_2, respectively. Combined relative uncertainty in the mole fraction of CO_2 was thus measured taking into consideration the relative uncertainties in the densities and volumes of water and CO_2. Using the above equation, the uncertainties in the CO_2 mole fractions, $x=(0.0118, 0.0066$ and $0.0015)$ were evaluated to be $u(x)=(0.0004, 0.0002$ and $0.0001)$, respectively.

5 Evaluation of Uncertainties

The overall standard uncertainties in sound speeds were evaluated using the following relation:

$$u_c(c) = \sqrt{\left(u(c)\right)^2 + \left(\frac{\partial c}{\partial T} \bullet u(T)\right)^2 + \left(\frac{\partial c}{\partial p} \bullet u(p)\right)^2 + \left(\frac{\partial c}{\partial x} \bullet u(x)\right)^2}. \quad (4)$$

The first term on the right-hand-side refers to the uncertainty in sound speed measurement, which is evaluated by taking into consideration the uncertainty of the acoustic path length difference, ΔL, and the uncertainty of time measurement, Δt. The second and third terms refer to influence of temperature and pressure, whereas the final term pertains to the influence of mixture composition. The partial derivatives (sensitivity coefficients) for uncertainty evaluation were obtained using the correlation of Eq. 5 discussed later. In this way, the maximum overall standard uncertainties were evaluated to be $u_c(c)=0.70$ m·s^{-1}, 0.39 m·s^{-1} and 0.13 m·s^{-1} for each mixture composition $x=0.0118, 0.0066$ and 0.0015, respectively, which

Table 4 Uncertainty budget for sound speed measurements in $0.0066 \cdot CO_2 + 0.9934 \cdot H_2O$ mixture at $T = 293.24$ K and $p = 20.00$ MPa, where $c = 1522.65$ (m·s^{-1})

Source	Standard uncertainty $u(i)$	Contribution to uncertainty $u(c)$ / m·s^{-1}
Temperature $u(T)$	20 mK	0.04
Pressure $u(p)$	8 kPa	0.03
Composition $u(x)$	0.0002	0.17
Sound speed measurement, $u(c)$	–	0.12
Overall combined standard uncertainty, $u_c(c)$		0.21

corresponds to relative standard uncertainties of 0.05 %, 0.03 % and 0.01 %. Standard uncertainties for each state point are provided next to the experimental sound speed values in Sect. 6. An uncertainty budget for sound speeds for an example case for $x = 0.0066$ mixture is presented in Table 4.

6 Experimental Results

A total of 402 experimental sounds speeds including repeat measurements were made over three binary mixtures $x \cdot CO_2 + (1 - x) \cdot H_2O$ with compositions $x = 0.0118$, 0.0066, and 0.0015 between temperatures of (273.15 and 313.15) K and pressures up to 50 MPa. All measured sound speed data with the standard uncertainties are provided in Tables 5, 6 and 7. At each composition, a total of 134 measurements were made with repeat measurements to confirm reproducibility. Reproducibility was tested by preparing a new mixture of CO_2 mole fraction $x = 0.0016$, with the results compared against the $x = 0.0015$ composition. At these compositions, the uncertainty in mole fraction of CO_2 is $u(x) = 0.0001$. The maximum difference between the sound speeds at $p = 10$ MPa, 30 MPa, 35 MPa and 40 MPa and at $T = 298$ K between these compositions was found to be less than 0.02 %.

The $x \cdot CO_2 + (1 - x) \cdot H_2O$ experimental sound speed data and selected experimental data for pure water ($x = 0$) of Lin and Trusler [33], Benedetto et al. [37] and Fujii [38] were fitted as functions of temperature, pressure and mole fraction of CO_2, i.e. $c = f(t,p,x)$ by means of Eq. 5 by minimizing the sum of squared residuals.

$$\frac{c_{fit}}{\left(10^3 m \bullet s^{-1}\right)} = \left[\sum_{i=0}^{2} \sum_{j=0}^{2} \sum_{k=0}^{1+\delta(j)} a_{ijk} t^i \varphi^j x^k \right]^{1/3} \tag{5}$$

In the above equation, $\varphi = p/\mathrm{GPa}$ and $t = (T/\mathrm{K}) - 273.15$ are dimensionless variables and $\delta(j) = 1$ for $j = 0$, and otherwise 0 (zero). In order to enforce agreement with the IAPWS-95 [29] EoS for pure water at low pressure, the three parameters a_{i00} ($i = 0, 1, 2$) were fitted to speeds of sound calculated from that model for metastable liquid water at zero pressure and at temperatures between 273.15 K and 303.15 K. The chosen functional form was found to represent the IAPWS-95 sound speeds with relative absolute deviations below 0.01 %. The remaining 16 parameters were fitted to the experimental data from both the present study and the selected literature

Table 5 Measured speeds of sound c and combined standard uncertainty $u_c(c)$ as a function of pressure p and temperature T for the mixture $0.0118 \cdot CO_2 + 0.9882 \cdot H_2O$

T/K	p/MPa	c/(m·s^{-1})	$u_c(c)$ /(m·s^{-1})
273.17	3.97	1433.28	0.70
273.19	5.97	1436.05	0.69
273.20	7.97	1438.84	0.68
273.23	9.97	1441.50	0.67
273.14	9.97	1441.25	0.67
273.13	11.95	1444.05	0.66
273.13	14.94	1448.15	0.64
273.13	17.93	1452.38	0.62
273.13	19.93	1455.33	0.61
273.13	24.92	1462.65	0.59
273.13	29.90	1470.03	0.57
273.12	34.89	1477.73	0.54
273.13	39.87	1485.39	0.52
273.13	44.85	1493.30	0.50
273.13	49.82	1501.26	0.48
278.12	3.63	1452.58	0.62
278.19	3.99	1453.50	0.62
278.22	5.99	1456.24	0.60
278.19	7.99	1459.12	0.59
278.18	9.98	1462.00	0.58
278.14	9.98	1462.00	0.59
278.14	11.98	1464.75	0.58
278.17	11.96	1464.84	0.57
278.19	14.93	1469.35	0.56
278.18	17.93	1473.80	0.55
278.17	19.92	1476.68	0.54
278.17	24.91	1484.21	0.52
278.16	27.90	1488.81	0.51
278.16	29.90	1491.85	0.50
278.16	34.88	1499.39	0.48
278.15	39.86	1507.17	0.46
278.15	44.84	1515.13	0.44
278.15	49.82	1523.13	0.43
283.18	3.99	1472.01	0.54
283.18	4.99	1473.63	0.53
283.18	7.99	1477.97	0.52
283.20	9.99	1480.84	0.51
283.19	11.95	1483.93	0.50
283.19	14.96	1488.38	0.49
283.17	17.93	1492.84	0.48
283.18	19.94	1495.84	0.47
283.19	24.90	1503.55	0.45
283.19	29.89	1511.23	0.44

Table 5 (continued)

T/K	p/MPa	c/(m·s^{-1})	$u_c(c)$ /(m·s^{-1})
283.18	34.86	1518.99	0.42
283.19	44.80	1534.80	0.39
283.19	49.78	1542.81	0.38
288.21	4.99	1489.28	0.46
288.21	5.97	1490.72	0.45
288.21	7.98	1493.89	0.44
288.21	9.97	1496.89	0.44
288.21	9.98	1497.01	0.44
288.21	11.96	1500.13	0.43
288.21	17.93	1509.31	0.41
288.21	14.94	1504.63	0.42
288.22	19.93	1512.43	0.41
288.22	24.90	1520.14	0.39
288.22	29.88	1528.09	0.38
288.22	34.86	1535.93	0.37
288.22	39.84	1543.81	0.36
288.22	44.81	1551.76	0.34
288.23	49.78	1559.64	0.33
293.21	5.99	1505.04	0.38
293.21	7.98	1508.15	0.38
293.22	9.95	1511.42	0.37
293.20	9.98	1511.15	0.37
293.21	11.95	1514.42	0.37
293.22	14.94	1519.16	0.36
293.22	17.93	1523.96	0.35
293.22	19.93	1527.07	0.35
293.22	24.91	1534.94	0.34
293.23	29.89	1542.93	0.33
293.22	29.89	1542.90	0.33
293.22	34.87	1550.81	0.32
293.22	39.85	1558.87	0.31
293.23	44.82	1566.82	0.30
293.23	49.79	1574.82	0.29
298.21	5.50	1516.91	0.33
298.21	7.50	1520.12	0.32
298.22	9.96	1524.07	0.32
298.22	9.99	1524.18	0.31
298.24	14.95	1532.16	0.31
298.22	19.95	1540.05	0.30
298.21	24.95	1548.15	0.30
298.25	29.94	1556.31	0.29
298.25	34.88	1564.31	0.28
298.21	39.88	1572.30	0.27

Table 5 (continued)

T/K	p/MPa	c/(m·s^{-1})	$u_c(c)$ /(m·s^{-1})
298.38	44.81	1580.47	0.27
298.27	49.83	1588.42	0.26
303.24	6.09	1528.17	0.26
303.24	7.99	1531.38	0.27
303.24	9.98	1534.53	0.27
303.23	9.98	1534.33	0.27
303.24	11.95	1537.78	0.26
303.25	14.94	1542.65	0.26
303.25	17.93	1547.60	0.26
303.25	17.94	1547.57	0.26
303.25	19.93	1550.79	0.25
303.25	24.91	1559.07	0.25
303.25	29.90	1566.99	0.25
303.25	34.87	1575.31	0.25
303.26	39.85	1583.34	0.24
303.26	44.83	1591.35	0.24
303.26	49.80	1599.60	0.23
308.28	7.97	1540.17	0.23
308.27	9.97	1543.80	0.23
308.26	11.95	1546.89	0.22
308.22	14.94	1551.71	0.22
308.22	17.94	1556.81	0.21
308.23	19.93	1560.03	0.21
308.23	24.92	1568.64	0.21
308.23	29.90	1576.80	0.21
308.24	34.89	1584.82	0.21
308.25	39.87	1592.97	0.21
308.25	44.85	1601.28	0.20
308.24	44.87	1601.24	0.20
308.25	49.82	1609.40	0.20
313.24	7.66	1547.30	0.20
313.24	7.71	1547.31	0.20
313.21	7.74	1547.42	0.18
313.23	7.99	1547.84	0.18
313.22	8.20	1548.23	0.18
313.24	9.98	1551.25	0.18
313.21	9.99	1551.21	0.18
313.25	14.97	1559.74	0.18
313.25	19.96	1568.16	0.18
313.21	20.00	1568.08	0.18
313.22	24.98	1576.45	0.18
313.26	29.94	1584.89	0.18
313.23	34.94	1592.95	0.18

Table 5 (continued)

T/K	p/MPa	c/(m·s^{-1})	$u_c(c)$ /(m·s^{-1})
313.23	39.90	1601.47	0.18
313.23	44.89	1609.87	0.18
313.25	49.86	1617.95	0.18

Standard uncertainty of temperature $u(T)$: 20 mK, standard uncertainty of pressure, $u(p) = 8$ kPa and standard uncertainty of composition, $u(x) = 0.0004$ mol fraction

data for pure water at temperatures between 273.15 K and 303.15 K with pressures up to 50 MPa.

The coefficients of fit 'a' along with the summary of statistics of fit are provided in Table 8. The root mean square deviation (RMSD) of the fit is 0.016 % with average deviations and maximum deviations from the fitting data being 0.013 % and 0.051 %, respectively. Nearly 82 % of the data are fitted to within 0.02 % absolute deviations with nearly 99 % of the data falling under 0.04 % which indicates a very high quality of fit. This correlation is valid in the experimental range of this study between $T = (273$ and $314)$ K and $p = (4$ and $50)$ MPa at $0 \leq x \leq 0.0118$. The relative percentage deviations of the data used for fitting are presented as functions of sound speeds, c in Fig. 6.

Statistics of fit: $\Delta_{AARD} = 0.013$ %; $\Delta_{MARD} = 0.051$ %; RMSD $= 0.016$ %.

The experimental sound speeds are plotted as functions of pressure at all the experimental isotherms in Fig. 7, Fig. 8, and Fig. 9 for $x = (0.0118, 0.0066$ and $0.0015)$, respectively. At each composition, for the given experimental range, sound speeds show an almost linear dependence on pressure, while varying non-linearly with temperature and composition. Increase in temperature increases the sound speeds at constant pressure. These observations are consistent for all three compositions. The effect of change in composition CO_2 to sound speeds of the binary mixtures is discussed in the following section.

7 Discussion

When gaseous CO_2 equilibrates with water, more than 99 % of CO_2 existing in the aqueous phase mixture remains a dissolved gas, with the rest reacting into H_2CO_3, H^+, HCO_3^- and CO_3^{2-} [39]. To verify whether this dissociation or any change in mixture composition has any noticeable effect on the measured sound speeds, experimental measurements were carried out for the $x = 0.0066$ mixture at $p = 100$ bar and $T = 278.15$ K at 20-min intervals over a period of 72 h. It was found that the observed variation in the measured speed of sound during this period was commensurate to the variation in temperature inside the incubator. No additional variations were observed over this time, which could have been indicative of a change in mixture composition.

Table 6 Measured speeds of sound c and combined standard uncertainty $u_c(c)$ as a function of pressure p and temperature T for the mixture $0.0066 \cdot CO_2 + 0.9934 \cdot H_2O$

T/K	p/MPa	c/(m·s^{-1})	$u_c(c)$ /(m·s^{-1})
273.16	4.01	1422.71	0.39
273.16	6.01	1425.57	0.38
273.16	8.00	1428.44	0.38
273.16	8.00	1428.66	0.38
273.15	10.02	1431.11	0.37
273.17	10.05	1431.57	0.37
273.16	14.99	1438.32	0.36
273.18	18.00	1443.04	0.35
273.17	20.00	1446.08	0.35
273.19	24.99	1453.90	0.34
273.16	30.08	1462.19	0.33
273.16	35.00	1469.98	0.32
273.17	40.00	1478.13	0.31
273.17	45.07	1486.53	0.30
273.17	50.05	1494.93	0.29
278.18	4.02	1444.15	0.34
278.18	6.03	1448.02	0.34
278.18	8.04	1450.37	0.33
278.18	10.00	1453.70	0.33
278.17	12.02	1456.15	0.32
278.18	14.99	1461.41	0.32
278.19	18.00	1466.26	0.33
278.18	20.00	1469.11	0.31
278.17	25.00	1476.97	0.30
278.18	30.00	1484.96	0.29
278.18	35.01	1493.11	0.28
278.19	40.08	1501.40	0.27
278.19	45.05	1509.70	0.27
278.19	50.03	1517.85	0.26
283.19	4.01	1464.54	0.30
283.19	6.01	1467.36	0.30
283.20	8.02	1470.55	0.29
283.21	10.02	1473.15	0.29
283.21	12.02	1476.41	0.31
283.21	15.00	1481.02	0.29
283.19	15.00	1481.33	0.28
283.21	18.00	1485.70	0.28
283.21	20.00	1489.01	0.28
283.21	25.00	1496.92	0.27
283.21	30.00	1504.92	0.27
283.20	35.01	1513.14	0.26
283.20	39.98	1521.31	0.25
283.19	45.00	1529.65	0.25

Table 6 (continued)

T/K	p/MPa	c/(m·s^{-1})	$u_c(c)$ /(m·s^{-1})
283.19	50.00	1537.96	0.24
287.99	4.02	1480.87	0.24
287.99	6.01	1484.04	0.27
288.00	8.00	1487.09	0.26
288.21	10.03	1490.59	0.26
288.02	10.02	1490.24	0.26
288.21	12.01	1494.04	0.26
288.21	15.00	1498.91	0.25
288.21	18.00	1503.50	0.25
288.21	20.00	1506.68	0.25
288.21	25.00	1514.78	0.24
288.20	30.00	1522.72	0.24
288.20	30.00	1522.78	0.23
288.19	35.00	1531.00	0.23
288.18	39.98	1539.04	0.23
288.14	44.97	1547.21	0.22
288.11	50.01	1555.29	0.22
293.21	4.02	1496.61	0.22
293.20	6.02	1499.78	0.23
293.20	8.02	1503.07	0.23
293.22	10.03	1506.22	0.22
293.20	10.01	1506.16	0.22
293.23	15.01	1514.33	0.22
293.23	18.00	1519.19	0.22
293.23	20.00	1522.65	0.22
293.23	24.99	1530.60	0.21
293.24	30.00	1538.79	0.21
293.21	30.01	1538.72	0.21
293.23	34.97	1546.85	0.21
293.21	40.00	1555.10	0.20
293.22	45.07	1563.45	0.20
293.22	50.04	1571.50	0.20
298.21	4.02	1510.04	0.20
298.21	5.00	1511.52	0.20
298.21	6.01	1513.05	0.20
298.21	8.01	1516.36	0.20
298.21	10.00	1519.50	0.20
298.22	9.99	1519.60	0.20
298.19	15.02	1527.84	0.20
298.19	18.00	1532.45	0.19
298.19	20.01	1535.79	0.19
298.19	20.01	1535.88	0.19
298.19	24.99	1543.95	0.19

Table 6 (continued)

T/K	p/MPa	c/(m·s^{-1})	$u_c(c)$ /(m·s^{-1})
298.17	29.95	1552.09	0.19
298.17	29.99	1552.11	0.19
298.17	34.93	1560.62	0.19
298.18	39.91	1568.49	0.18
298.18	44.99	1577.07	0.18
298.18	50.06	1585.28	0.18
303.23	5.01	1522.15	0.18
303.22	6.01	1524.13	0.17
303.22	8.02	1527.58	0.17
303.22	9.02	1529.16	0.17
303.22	10.02	1530.89	0.17
303.22	15.02	1539.19	0.17
303.22	18.02	1544.27	0.17
303.23	25.05	1555.79	0.17
303.23	30.08	1564.07	0.17
303.24	34.96	1572.35	0.17
303.24	39.94	1580.45	0.17
303.25	44.95	1589.02	0.17
303.25	49.94	1597.17	0.17
308.26	5.02	1532.39	0.17
308.25	8.02	1537.47	0.15
308.33	10.01	1541.00	0.15
308.25	10.04	1540.81	0.15
308.28	15.00	1549.62	0.15
308.29	18.02	1554.44	0.15
308.30	20.00	1557.67	0.15
308.29	24.96	1565.98	0.15
308.28	29.95	1574.73	0.15
308.27	34.93	1582.63	0.16
308.27	39.92	1591.05	0.16
308.27	44.97	1599.21	0.16
308.27	50.04	1608.22	0.16
313.27	5.01	1540.53	0.16
313.27	6.02	1542.60	0.14
313.27	8.02	1545.53	0.14
313.31	10.01	1548.98	0.14
313.27	10.01	1549.32	0.14
313.29	12.01	1552.52	0.14
313.29	15.00	1557.96	0.14
313.29	18.01	1562.73	0.14
313.30	20.00	1565.96	0.14
313.30	25.00	1574.99	0.14
313.31	30.00	1583.09	0.14

Table 6 (continued)

T/K	p/MPa	c/(m·s^{-1})	u$_c$(c) /(m·s^{-1})
313.31	35.00	1591.53	0.14
313.31	40.01	1599.81	0.15
313.31	44.97	1608.37	0.15
313.31	50.04	1617.16	0.15

Standard uncertainty of temperature $u(T)$: 20 mK, standard uncertainty of pressure, $u(p) = 8$ kPa and standard uncertainty of composition, $u(x) = 0.0002$ mol fraction

The relative differences between sound speeds in all compositions of the $x CO_2 + (1 - x) \cdot H_2O$ mixture and pure water are presented in Fig. 10 as functions of pressure for various experimental isotherms. In general, sound speeds increase when more CO_2 is added to water (higher concentration). The increase in sound speeds for mixtures of CO_2 and water, compared to pure water, is due to the decrease in compressibility of the mixture. When CO_2 is dissolved in water, a cage-like structure of H_2O molecules forms around the CO_2 molecule [40] increasing the rigidity of the local structure, i.e., making it less compressible [41]. At the experimental conditions, maximum increases in sound speeds of up to 25 m/s, 15 m/s and 2 m/s were observed for the compositions, $x = (0.0118, 0.0066$ and $0.0015)$, respectively. For the two higher concentrations of CO_2, there is a clear decrease in sound speed differences with increasing temperature. For the lowest CO_2 composition, the magnitude of the variation is not as large, differing from pure water between 0.4 m/s and 2 m/s. Although small, the change is experimentally significant considering that the maximum estimated standard uncertainty at this composition is less than 0.2 m/s.

In Fig. 11, speeds of sound for each mixture are plotted as a function of pressure at $T = 298.15$, along with the prediction for pure water using IAPWS-95 [29] and predictions for each mixture based on the EOS of Gernert and Span [10]. The EOS consistently over-predicts the sound speeds of the mixtures by a significant amount. For example, for the $x = 0.0118$ composition, the EOS predicted sound speeds are consistently higher than our experimental results by more than 80 m/s. The differences reduce to about 10 m/s at the lowest concentration of CO_2 ($x = 0.0015$). These significant differences in the predictions by the EOS could potentially be due to the fact that it was developed for humid gases and CO_2 and not for pure water and CO_2 mixture. Additionally, there is limited available accurate experimental data for the $x \cdot CO_2 + (1 - x) \cdot H_2O$ that could be used for fitting.

To our knowledge, there is very limited experimental sound speed data available in the literature for $x \cdot CO_2 + (1 - x) \cdot H_2O$ mixtures. Sanemasa et al. [11] present some values of experimental sound speed differences from pure water for mixtures at low concentrations of $x = (0.002$ to $0.005)$, at pressures less than 1 MPa and at temperatures between $T = (295$ and $302)$ K. Since these pressures are much lower than our experimental pressure conditions, a comparison with their data were carried out by extrapolating the correlation of Eq. 5 to the low-pressure conditions. The comparison between our fitted results and the experimental results of Sanemasa et al. [11] is shown in Fig. 12. Taking water as a reference, the deviation in sound speeds agree

Table 7 Measured speeds of sound c and combined standard uncertainty $u_c(c)$ as a function of pressure p and temperature T for the mixture $0.0015 \cdot CO_2 + 0.9985 \cdot H_2O$

T/K	p/MPa	$c/(m \cdot s^{-1})$	$u_c(c)/(m \cdot s^{-1})$
273.18	4.00	1410.64	0.16
273.18	6.00	1413.88	0.15
273.20	8.00	1417.21	0.16
273.24	9.98	1420.23	0.15
273.23	10.00	1420.22	0.16
273.24	15.00	1428.15	0.15
273.18	17.96	1432.63	0.15
273.24	19.98	1436.17	0.15
273.23	24.99	1444.42	0.15
273.24	29.93	1452.73	0.15
273.24	35.00	1461.32	0.15
273.18	40.00	1469.65	0.15
273.17	40.02	1469.71	0.15
273.23	44.97	1478.40	0.16
273.20	50.05	1487.48	0.15
278.22	3.99	1434.67	0.15
278.23	5.99	1437.71	0.14
278.23	7.99	1440.82	0.15
278.24	9.99	1444.04	0.15
278.25	12.00	1447.27	0.15
278.25	15.00	1452.25	0.14
278.23	19.99	1460.26	0.15
278.26	20.00	1460.37	0.15
278.20	25.02	1468.33	0.15
278.22	30.00	1476.81	0.15
278.21	35.00	1485.03	0.15
278.22	39.99	1493.73	0.15
278.21	40.01	1493.59	0.15
278.21	44.98	1502.25	0.15
278.22	49.94	1510.93	0.15
283.19	4.01	1455.41	0.14
283.18	6.00	1458.52	0.14
283.16	7.99	1461.63	0.14
283.15	9.99	1464.68	0.14
283.20	11.99	1468.18	0.14
283.14	15.00	1472.86	0.14
283.13	18.00	1477.81	0.14
283.11	20.00	1480.87	0.14
283.09	25.03	1489.14	0.14
283.22	29.99	1497.99	0.14
283.17	29.99	1497.96	0.14
283.06	35.04	1505.95	0.14
283.09	39.98	1514.57	0.15

Table 7 (continued)

T/K	p/MPa	c/(m·s^{-1})	$u_c(c)$ /(m·s^{-1})
283.05	45.00	1522.89	0.15
283.07	49.93	1531.32	0.15
288.31	4.00	1474.38	0.13
288.27	6.01	1477.42	0.13
288.25	7.99	1480.62	0.13
288.29	9.99	1484.04	0.13
288.20	12.01	1486.83	0.13
288.25	14.99	1492.03	0.13
288.25	18.00	1497.04	0.13
288.18	20.00	1500.27	0.13
288.17	20.01	1499.98	0.13
288.13	25.01	1508.05	0.13
288.11	30.02	1516.36	0.14
288.10	35.06	1524.87	0.14
288.09	40.01	1533.18	0.14
288.09	40.03	1533.02	0.14
288.09	45.00	1541.55	0.14
288.09	49.96	1550.10	0.15
293.24	4.01	1490.21	0.13
293.24	6.00	1493.66	0.13
293.24	8.00	1496.99	0.13
293.24	9.99	1500.24	0.13
293.23	11.99	1503.48	0.13
293.25	14.99	1508.47	0.13
293.23	18.00	1513.34	0.13
293.23	20.00	1516.85	0.13
293.24	25.02	1525.15	0.13
293.24	30.00	1533.43	0.13
293.24	35.01	1541.71	0.13
293.25	40.00	1550.20	0.14
293.24	40.01	1550.17	0.14
293.25	44.99	1558.55	0.14
293.25	50.00	1567.24	0.14
298.26	4.01	1504.65	0.12
298.26	6.01	1507.93	0.12
298.26	8.00	1511.30	0.12
298.26	10.00	1514.65	0.12
298.26	15.01	1522.90	0.12
298.26	18.01	1527.97	0.13
298.24	20.01	1531.19	0.13
298.27	19.99	1531.23	0.13
298.24	25.00	1539.51	0.13
298.22	29.99	1548.04	0.13

Table 7 (continued)

T/K	p/MPa	c/(m·s^{-1})	$u_c(c)$ /(m·s^{-1})
298.23	34.99	1556.27	0.13
298.25	35.00	1556.34	0.13
298.23	40.01	1564.86	0.13
298.24	40.00	1564.76	0.13
298.24	45.08	1573.38	0.14
298.25	49.96	1581.58	0.14
303.24	4.01	1516.83	0.12
303.23	6.01	1520.15	0.12
303.23	8.01	1523.60	0.12
303.29	10.00	1526.93	0.13
303.23	10.01	1526.96	0.12
303.24	14.97	1535.30	0.12
303.24	17.96	1540.37	0.12
303.25	20.03	1543.94	0.13
303.25	25.04	1552.20	0.13
303.32	30.00	1560.90	0.13
303.29	35.00	1569.39	0.13
303.29	40.00	1577.76	0.13
303.27	40.03	1577.68	0.13
303.29	44.98	1586.03	0.14
303.28	49.96	1594.51	0.14
308.27	4.01	1527.40	0.11
308.28	6.01	1530.94	0.12
308.28	8.01	1534.26	0.12
308.27	10.00	1537.65	0.12
308.29	9.97	1537.58	0.12
308.29	14.98	1546.27	0.12
308.30	17.96	1551.22	0.12
308.28	20.00	1554.79	0.12
308.30	25.01	1563.29	0.12
308.27	29.98	1571.55	0.13
308.30	30.01	1571.59	0.13
308.25	34.99	1580.18	0.13
308.27	39.99	1588.61	0.13
308.31	44.98	1597.11	0.13
308.29	49.94	1605.49	0.14
313.30	4.01	1536.30	0.12
313.30	6.01	1539.89	0.12
313.30	8.01	1543.50	0.12
313.33	9.99	1546.88	0.12
313.29	9.99	1546.80	0.12
313.29	15.00	1555.47	0.12
313.31	14.99	1555.43	0.12

Table 7 (continued)

T/K	p/MPa	c/(m·s^{-1})	$u_c(c)$ /(m·s^{-1})
313.33	19.99	1564.13	0.12
313.30	25.00	1572.67	0.13
313.32	29.99	1581.27	0.13
313.30	30.00	1581.34	0.13
313.30	34.99	1589.74	0.13
313.33	39.99	1598.14	0.16
313.32	44.99	1606.67	0.15
313.33	50.05	1615.12	0.16

Standard uncertainty of temperature $u(T)$: 20 mK, standard uncertainty of pressure, $u(p) = 8$ kPa and standard uncertainty of composition, $u(x) = 0.0001$ mol fraction

Table 8 Values of parameters of correlation of Eq. 5 with statistics of fit

a_{000}	a_{001}	a_{002}	a_{010}	a_{011}	a_{012}	a_{020}
2.757509	13.811998	-83.955510	0.029487	-0.252501	-2.584396	-0.000228
a_{021}	a_{022}	a_{100}	a_{101}	a_{102}	a_{110}	a_{111}
-0.000271	0.105613	8.526854	-19.941189	0	0.104486	1.309579
a_{112}	a_{120}	a_{121}	a_{122}	a_{300}	a_{301}	a_{302}
0	-0.000387	-0.013999	0	36.348981	-933.148602	0
a_{310}	a_{311}	a_{312}	a_{320}	a_{321}	a_{322}	
-0.649073	14.314462	0	0	0	0	
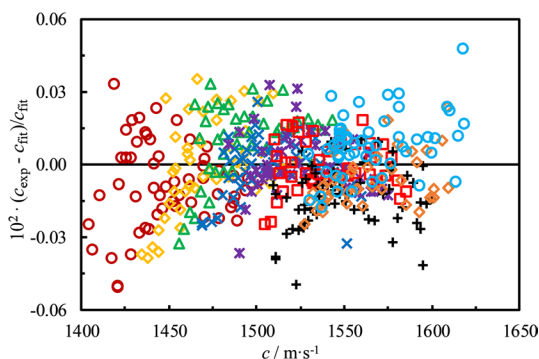
Fig. 6 Relative percentage deviations of experimental sound speeds in selected pure water data of Lin and Trusler [33], Benedetto et al. [37] and Fujii [38] and in binary x·CO$_2$ + (1 − x)·H$_2$O mixtures measured in this work, c_{exp}, from the correlation sound speeds, c_{fit} of Eq. 5 as functions of sound speeds at various experimental isotherms, T. ○, $T = 273$ K; ◇, $T = 278$ K; △, $T = 283$ K; ×, $T = 288$ K; ✳, $T = 293$ K; □, $T = 298$ K; +, $T = 303$ K; ◇, $T = 308$ K; ○, $T = 313$ K

Fig. 7 Experimental speeds of sound in $0.0118 \cdot CO_2 + 0.9882 \cdot H_2O$ mixture, c_{exp}, as a function of pressure. $\diamondsuit$, $T = 273.15$ K; $\bigcirc$, $T = 278.17$ K; $\triangle$, $T = 283.19$ K; $\diamondsuit$, $T = 288.21$ K; $*$, $T = 293.22$ K; $\square$, $T = 298.24$ K; $\triangle$, $T = 303.25$ K; $+$, $T = 308.24$ K; $\bigcirc$, $T = 313.23$ K. Solid lines represent the correlated values of sound speeds in the mixture evaluated using Eq. 5
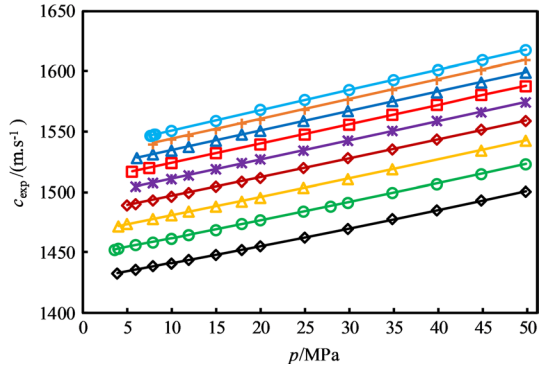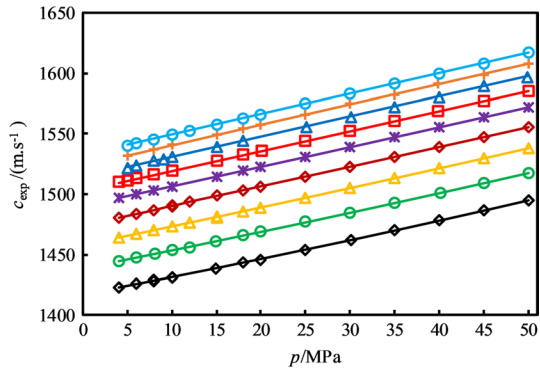

Fig. 8 Experimental speeds of sound in $0.0066 \cdot CO_2 + 0.9934 \cdot H_2O$ mixture, c_{exp}, as a function of pressure. $\diamondsuit$, $T = 273.17$ K; $\bigcirc$, $T = 278.18$ K; $\triangle$, $T = 283.20$ K; $\diamondsuit$, $T = 288.14$ K; $*$, $T = 293.22$ K; $\square$, $T = 298.19$ K; $\triangle$, $T = 303.23$ K; $+$, $T = 308.28$ K; $\bigcirc$, $T = 313.29$ K. Solid lines represent the correlated values of sound speeds in the mixture evaluated using Eq. 5

Fig. 9 Experimental speeds of sound in $0.0015 \cdot CO_2 + 0.9985 \cdot H_2O$ mixture, c_{exp}, as a function of pressure. $\diamondsuit$, $T = 273.21$ K; $\bigcirc$, $T = 278.23$ K; $\triangle$ $T = 283.18$ K; $\diamondsuit$, $T = 288.18$ K; $*$, $T = 293.24$ K; $\square$, $T = 298.25$ K; $\triangle$, $T = 303.26$ K; $+$, $T = 308.28$ K; $\bigcirc$, $T = 313.31$ K. Solid lines represent the correlated values of sound speeds in the mixture evaluated using Eq. 5
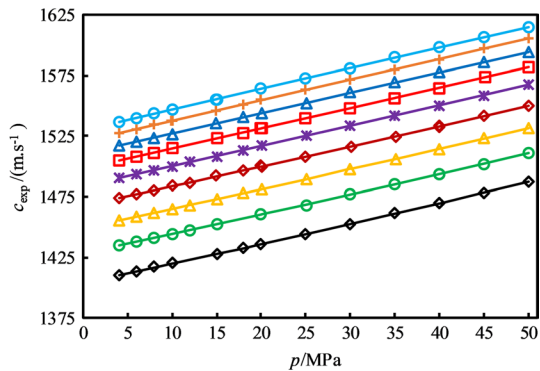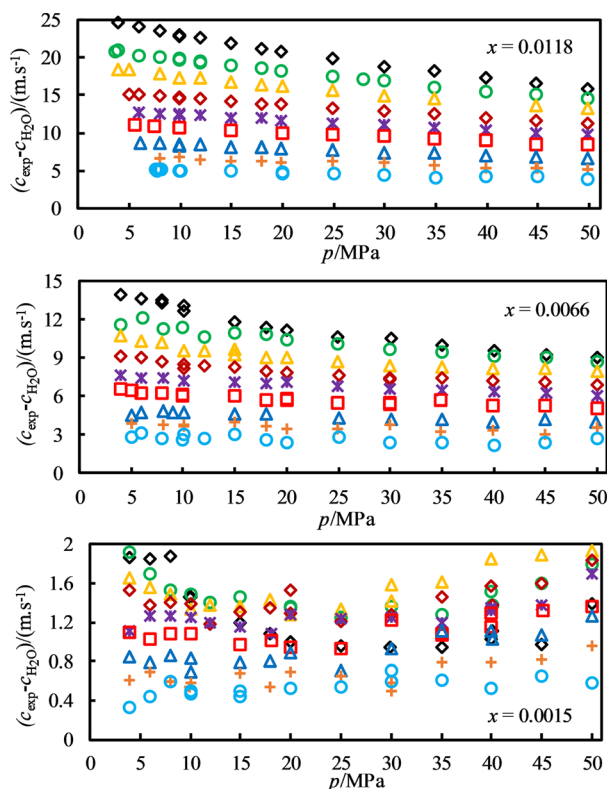
Fig. 10 Differences of sound speeds in various compositions of mixture $x{\cdot}CO_2+(1-x){\cdot}H_2O$, c_{exp}, compared to the sound speeds in pure water, c_{H2O} evaluated using IAPWS-95 [29] as functions of pressure at various temperatures. $\diamond$, $T=273.15$ K; $\bigcirc$, $T=278.17$ K; $\triangle$, $T=283.19$ K; $\diamond$, $T=288.21$ K; $*$, $T=293.22$ K; $\square$, $T=298.24$ K; $\triangle$, $T=303.25$ K; $+$, $T=308.24$ K; $\bigcirc$, $T=313.23$ K

well with our results, with maximum difference between the results being less than 0.03 %. In these conditions, their results and ours indicate a maximum difference of about 5 m/s in sound speed compared to water. However, the predictions of the EOS of Gernert and Span [10] (see Fig. 12), vary from our predictions by as much as 2 %. In these low concentrations, the EOS seems to be over-estimating the influence of additional CO_2 in water for sound speed. Over the entire experimental range of this study, our experimental data deviate from the EOS by up to 7 %.

8 Conclusions

Speeds of sound in binary mixtures of $x{\cdot}CO_2+(1-x){\cdot}H_2O$ for $x=(0.0118, 0.0066$ and $0.0015)$ are reported, measured using the double-path pulse-echo apparatus at temperatures between $T=273.15$ K and 313.15 K and pressures up to
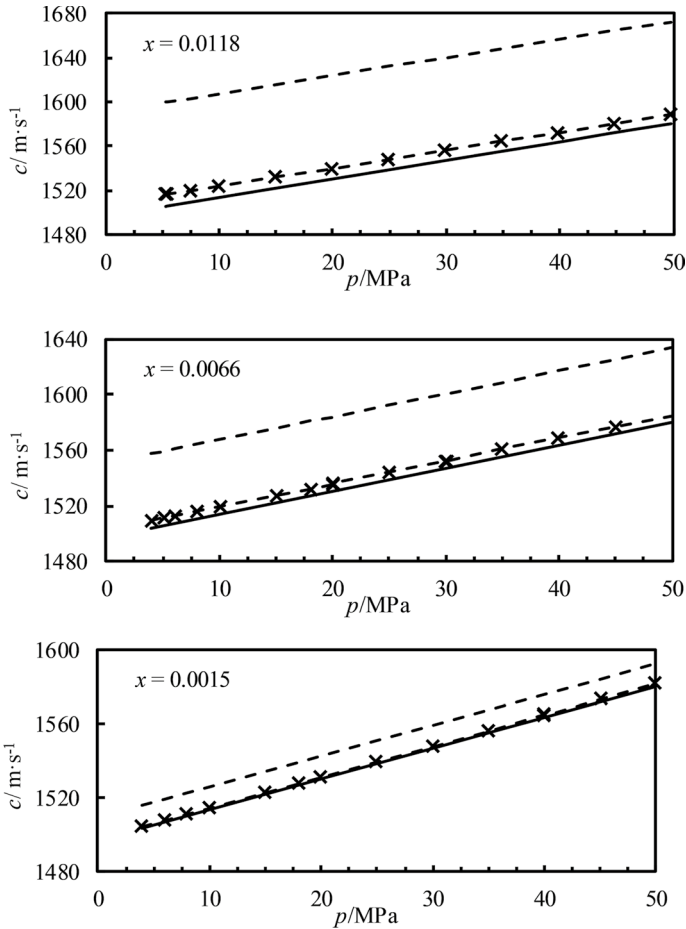
Fig. 11 Speeds of sound in $x \cdot CO_2 + (1-x) \cdot H_2O$ mixture and pure water as functions of pressure at $T = 298.15$ K. −×−, This work; – –, Gernert and Span[10]; —— IAPWS-95 [29]

50 MPa. The standard uncertainties of our experimental data are at most 0.97 m/s, 0.55 m/s and 0.19 m/s for compositions, $x = (0.0118, 0.0066$ and $0.0015)$, respectively. The results were compared against limited experimental data and the latest EOS. Our results agree well to within 0.03 % of the experimental data, whereas they deviate by up to 7 % from the EOS. Our results show greatest deviations from the EOS at the lowest temperature and highest pressure of the higher mole fractions of CO_2. The large discrepancies may be due to the limited experimental data that was available for these mixtures during EOS development. The accurate experimental sound speeds reported here can be used to improve the predictions
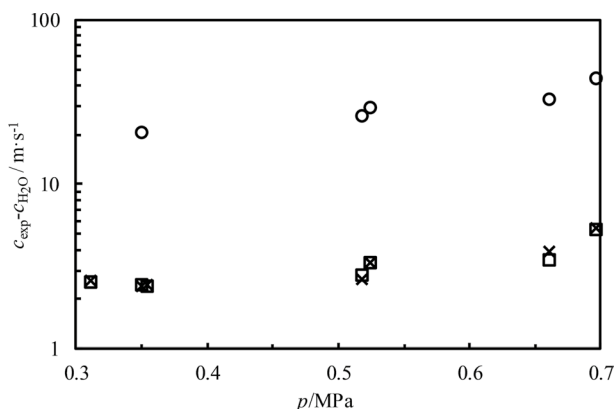
Fig. 12 Deviations of sound speeds in $x \cdot CO_2 + (1 - x) \cdot H_2O$ from sound speeds in pure water evaluated using IAPWS-95[29] at various compositions between $x = (0.002$ and $0.005)$ and temperatures between $T = 295$ K and 302 K as functions of pressure. Sound speed deviations in water from: □, This work, ×, Sanemasa et al.[11]; ○, EOS of Gernert and Span [10]

of the EOS for the $x \cdot CO_2 + (1 - x) \cdot H_2O$, particularly at low concentrations of CO_2 (i.e., at $x < 0.01$). Additionally, our experimental sound speeds can be potentially analysed to obtain other important thermodynamic properties including heat capacity, density and compressibility when used in conjunction with accurate density and heat capacity data at reference conditions. Combined with ongoing experimental work to measure sound speed for the ternary mixtures of H_2O with CO_2 and NaCl, these data and improvements to associated EOSs have the potential to improve the accuracy of climate models.

Data Availability N/A.

Code Availability N/A.

Declarations

Conflict of interest There are no relevant financial or non-financial conflicts of interest or competing interests to report.

Ethical Approval N/A.

Consent to Participate N/A.

Consent for Publication N/A.

References

1. J. Hu et al., PVTx properties of the CO_2–H_2O and CO_2–H_2O–NaCl systems below 647 K: assessment of experimental data and thermodynamic models. Chem. Geol. **238**(3–4), 249–267 (2007)
2. J.P.M. Trusler, Thermophysical properties and phase behavior of fluids for application in carbon capture and storage processes. Annu. Rev. Chem. Biomol. Eng. **8**(1), 381–402 (2017)
3. Y.J. Lim et al., Seawater desalination by reverse osmosis: Current development and future challenges in membrane fabrication—a review. J. Membr. Sci. **629**, 119292 (2021)
4. K.G. Nayar et al., Thermophysical properties of seawater: a review and new correlations that include pressure dependence. Desalination **390**, 1–24 (2016)
5. T.W. Seow et al., Review on wastewater treatment technologies. Int. J. Appl. Environ. Sci **11**(1), 111–126 (2016)
6. F.J. Millero et al., The composition of standard seawater and the definition of the reference-composition salinity scale. Deep Sea Res. Part I **55**(1), 50–72 (2008)
7. Y. Kaya, M. Yamaguchi, K. Akimoto, The uncertainty of climate sensitivity and its implication for the Paris negotiation. Sustain. Sci. **11**(3), 515–518 (2016)
8. J. Bjordal et al., Equilibrium climate sensitivity above 5 °C plausible due to state-dependent cloud feedback. Nat. Geosci. **13**(11), 718–721 (2020)
9. S. Levitus, J. Antonov, T. Boyer, Warming of the world ocean, 1955–2003. Geophys. Res. Lett. **32**(2), L02604 (2005)
10. J. Gernert, R. Span, EOS–CG: a Helmholtz energy mixture model for humid gases and CCS mixtures. J. Chem. Thermodyn. **93**, 274–293 (2016)
11. M. Sanemasa et al., A new method to determine dissolved CO_2 concentration of lakes Nyos and Monoun using the sound speed and electrical conductivity of lake water. Geol. Soc. Lond. Spec. Publ. **437**(1), 193 (2017)
12. J.A. Nighswander, N. Kalogerakis, A.K. Mehrotra, Solubilities of carbon dioxide in water and 1 wt% sodium chloride solution at pressures up to 10 MPa and temperatures from 80 to 200°C. J. Chem. Eng. Data **34**(3), 355–360 (1989)
13. A. Fenghour, W.A. Wakeham, J.T.R. Watson, Densities of (water + carbon dioxide) in the temperature range 415 K to 700 K and pressures up to 35 MPa. J. Chem. Thermodyn. **28**(4), 433–446 (1996)
14. L. Hnědkovský et al., Volumes of aqueous solutions of CH_4, CO_2, H_2S and NH_3 at temperatures from 298.15 K to 705 K and pressures to 35 MPa. J. Chem. Thermodyn. **28**(2), 125–142 (1996)
15. Y. Song et al., Measurement on CO_2 solution density by optical technology. J. Vis. **6**(1), 41–51 (2003)
16. Z. Li et al., Densities and solubilities for binary systems of carbon dioxide + water and carbon dioxide + brine at 59 °C and pressures to 29 MPa. J. Chem. Eng. Data **49**(4), 1026–1031 (2004)
17. A. Hebach, A. Oberhof, N. Dahmen, Density of water+ carbon dioxide at elevated pressures: measurements and correlation. J. Chem. Eng. Data **49**(4), 950–953 (2004)
18. M. McBride-Wright, G.C. Maitland, J.P.M. Trusler, Viscosity and density of aqueous solutions of carbon dioxide at temperatures from (274 to 449) K and at pressures up to 100 MPa. J. Chem. Eng. Data **60**(1), 171–180 (2015)
19. E.C. Efika et al., Saturated phase densities of (CO_2 + H_2O) at temperatures from (293 to 450)K and pressures up to 64MPa. J. Chem. Thermodyn. **93**, 347–359 (2016)

20. J.A. Barbero et al., Thermodynamics of aqueous carbon dioxide and sulfur dioxide: heat capacities, volumes, and the temperature dependence of ionization. Can. J. Chem. **61**(11), 2509–2519 (1983)

21. L. Hnědkovský, R.H. Wood, Apparent molar heat capacities of aqueous solutions of CH_4, CO_2, H_2S, and NH_3 at temperatures from 304 K to 704 K at a pressure of 28 MPa. J. Chem. Thermodyn. **29**(7), 731–747 (1997)

22. H. Teng et al., Solubility of liquid CO_2 in water at temperatures from 278 K to 293 K and pressures from 6.44 MPa to 29.49 MPa and densities of the corresponding aqueous solutions. J. Chem. Thermodyn. **29**(11), 1301–1310 (1997)

23. P. Servio, P. Englezos, Effect of temperature and pressure on the solubility of carbon dioxide in water in the presence of gas hydrate. Fluid Phase Equilib. **190**(1), 127–134 (2001)

24. G.K. Anderson, Solubility of carbon dioxide in water under incipient clathrate formation conditions. J. Chem. Eng. Data **47**(2), 219–222 (2002)

25. S. Dhakal et al., Thermodynamic properties of liquid toluene from speed-of-sound measurements at temperatures from 283.15 K to 473.15 K and at pressures up to 390 MPa. Int. J. Thermophys. **42**(12), 169 (2021)

26. Z. Duan et al., An improved model for the calculation of CO_2 solubility in aqueous solutions containing Na^+, K^+, Ca^{2+}, Mg^{2+}, Cl^-, and SO_4^{2-}. Mar. Chem. **98**(2), 131–139 (2006)

27. S.Z.S. Al Ghafri et al., Speed of sound and derived thermodynamic properties of para-xylene at temperatures between (306 and 448) K and at pressures up to 66 MPa. J. Chem. Thermodyn. **135**, 369–381 (2019)

28. S.J. Ball, J.P.M. Trusler, Speed of sound of n-hexane and n-hexadecane at temperatures between 298 and 373 k and pressures up to 100 MPa. Int. J. Thermophys. **22**, 427–443 (2001)

29. W. Wagner, A. Pruß, The IAPWS formulation 1995 for the thermodynamic properties of ordinary water substance for general and scientific use. J. Phys. Chem. Ref. Data **31**(2), 387–535 (2002)

30. J.P. Hammond et al., *Dynamic and Static Measurements of Elastic Constants with Data on 2 1/4 Cr–1 Mo Steel, Types 304 and 316 Stainless Steels, and Alloy 800H* (Oak Ridge National Lab (ORNL), Oak Ridge, 1979)

31. H.M. Ledbetter, Stainless-steel elastic constants at low temperatures. J. Appl. Phys. **52**(3), 1587–1589 (1981)

32. M. Grujicic, H. Zhao, Optimization of 316 stainless steel/alumina functionally graded material for reduction of damage induced by thermal residual stresses. Mater. Sci. Eng. A **252**(1), 117–132 (1998)

33. C.W. Lin, J.P.M. Trusler, The speed of sound and derived thermodynamic properties of pure water at temperatures between (253 and 473) K and at pressures up to 400 MPa. J. Chem. Phys. **136**(9), 094511 (2012)

34. C.T. Chen, L.S. Chen, F.J. Millero, Speed of sound in NaCl, $MgCl_2$, Na_2SO_4, and $MgSO_4$ aqueous solutions as functions of concentration, temperature, and pressure. J. Acoust. Soc. Am. **63**(6), 1795–1800 (1978)

35. R. Span, W. Wagner, A new equation of state for carbon dioxide covering the fluid region from the triple-point temperature to 1100 K at pressures up to 800 MPa. J. Phys. Chem. Ref. Data **25**(6), 1509–1596 (1996)

36. S.Z.S. Al Ghafri et al., Thermodynamic properties of hydrofluoroolefin (R1234yf and R1234ze(E)) refrigerant mixtures: density, vapour-liquid equilibrium, and heat capacity data and modelling. Int. J. Refrig. **98**, 249–260 (2019)

37. G. Benedetto et al., Speed of sound in pure water at temperatures between 274 and 394 K and at pressures up to 90 MPa. Int. J. Thermophys. **26**, 1667–1680 (2005)

38. K. Fujii, *12th Symposium on Thermophysical Properties* (Plenum Press, Boulder, 1994)

39. W. Knoche, *Chemical Reactions of CO2 in Water* (Springer, Berlin, 1980)

40. K. Gilbert et al., CO_2 solubility in aqueous solutions containing Na^+, Ca^{2+}, Cl^-, SO_4^{2-} and HCO^{3-}: the effects of electrostricted water and ion hydration thermodynamics. Appl. Geochem. **67**, 59–67 (2016)

41. A. Burakowski, J. Gliński, Additivity of adiabatic compressibility with the size and geometry of the solute molecule. J. Mol. Liq. **137**(1), 25–30 (2008)

Publisher's Note Springer Nature remains neutral with regard to jurisdictional claims in published maps and institutional affiliations.

Authors and Affiliations

Subash Dhakal[1] · Saif Z. S. Al Ghafri[1] · Darren Rowland[1] · Eric F. May[1] · J. P. Martin Trusler[2] · Paul L. Stanwix[1]

✉ Paul L. Stanwix
   paul.stanwix@uwa.edu.au

[1]   Fluid Science & Resources Division, Department of Chemical Engineering, The University of Western Australia, Crawley, WA 6009, Australia

[2]   Department of Chemical Engineering, Imperial College London, London SW7 2AZ, UK